

Plug-In Hybrid Vehicle and Second-Life Applications of Lithium-Ion Batteries at Elevated Temperature

Rutvik Vaidya,^[a] Vishnu Selvan,^[a] Pavan Badami,^[a] Kathy Knoop,^[c] and Arunachala M. Kannan^{*[b]}

In improving fuel economy and reducing carbon footprint, hybrid, plug-in hybrid and all-electric vehicles are considered as sustainable modes of transportation in the automotive industry. Here, commercial Li-ion cells (26650 and 18650 with lithium iron phosphate (LFP) and nickel manganese cobalt (NMC) cathodes) were subjected to simulated plug-in hybrid electric vehicle (PHEV) conditions, using the Federal Urban Driving Schedule (FUDS) under charge-depleting mode at elevated temperature (50 °C and <10% RH). The capacity degradation (16% over 800 cycles) under the PHEV test protocol for Li-ion batteries with 26650 NMC cathodes was twice of that using LFP cathodes (8% over 800 cycles) under identical conditions. The Li-ion batteries were also subjected to second-life charge–discharge cycling at

C/5 rate after evaluating them under the PHEV protocol (800 cycles for 26650 cells and 1200 cycles for 18650 cells). In addition, the high-frequency resistance measured by electrochemical impedance spectroscopy was found to increase significantly with cycling for both the NMC- as well as LFP-based batteries, leading to power fading. XRD analysis of the 18650 LFP-based battery showed change of phase from LiFePO_4 to FePO_4 , indicating Li^+ -ion loss. However, the cathode active materials of the Li-ion cells (26650 with LFP and NMC cathodes), examined using XRD, showed no significant phase change in the materials after 800 PHEV cycles and around 200 second-life charge–discharge cycles.

1. Introduction

Fossil fuels have been the primary energy source for automotive applications due to their accessibility and affordability. As per the Intergovernmental Panel on Climate Change (IPCC), since 1970, CO_2 emissions have increased by about 90%, with emissions from fossil fuels and industrial processes contributing about 78% of the total greenhouse gases (GHG) emissions increase.^[1] In 2012, US consumed around 366 million gallons of gasoline per day, accounting for 66% of US transportation energy and 47% of US petroleum consumption. Electric Vehicles can potentially reduce the US gasoline consumption.^[2] As per an EPA report, in 2014, transportation accounted for 32% of the total CO_2 emissions in the United States.^[3] Climate change is being considered as a global crisis and countries are trying to reduce carbon dioxide emissions by shifting to cleaner fuels. However, some of these issues can be solved by using renewable sources of energy in the transportation sector, due of the increasing costs of fossil fuels and the environmental threats of GHGs. In this context, hybrid (HEV), plug-in hybrid (PHEV) and all-electric vehicles (EV) are being developed and

commercialized to reduce carbon footprint. For many electric vehicles, the ESS is the most expensive component of the vehicle, and hence it is important for the battery to last the life of the vehicle.^[2] According to the battery industry, the end-of-life (EOL) is the point where the battery's energy storage capacity drops by 20% of its initial value of when the impedance increases by 30%, whichever comes first.^[4] The PHEV technology is more advanced than HEV technology due to its ability to drive longer ranges using only electric power, because of smarter energy management algorithms and the convenience of recharging the battery pack with grid electricity.^[5] According to US Advanced Battery Consortium (USABC), in order to compete with the conventional internal combustion engine (ICE) based vehicles, a PHEV is targeted to have 15 years of calendar life, 5000 cycles of charge-depleting and 300000 cycles of charge-sustaining mode cycle life by 2018.^[6,7] Another target is to increase the specific energy and specific power values for batteries from 100 to 250 Wh/kg and 400 to 2000 W/kg, respectively.^[8]

LIBs can achieve highest gravimetric energy and power densities, and hence are preferred over other batteries for EVs. Another advantage of LIBs is the high capacity utilization even at high current rates, and hence these batteries are suitable for high current application such as EVs and PHEVs. Currently, EVs use Li-ion batteries due to better power and energy characteristics, and these can differ among different Li-ion batteries.^[9] The various types of intercalation cathode materials studied for Li-ion batteries can be classified as layered (LiCoO_2 , $\text{Li}(\text{Ni}-\text{Mn}-\text{Co})\text{O}_2$ and LiTiS_2), spinel (LiMn_2O_4 and LiCoO_2), olivine (LiFePO_4 and LiCoPO_4), and tavorite (LiFeSO_4F and LiVPO_4F) materials.^[10]

[a] R. Vaidya, V. Selvan, P. Badami

School for Engineering of Matter, Transport and Energy, Arizona State University, Tempe, AZ 85287, USA

[b] Prof. A. M. Kannan

The Polytechnic School, Ira A. Fulton Schools of Engineering, Arizona State University, Mesa, AZ 85212, USA

Phone: 480-7271102

E-mail: amk@asu.edu

[c] Dr. K. Knoop

Sustainability Policy and Programs, Salt River Project, Phoenix, AZ 85072, USA

The LiFePO₄ (LFP) based chemistries are extensively studied in public literature due to their safety and longer life, although these batteries have lower energy densities than some other Li-ion chemistries.^[6] LFP shows an excellent flat discharge voltage of 3.5 V vs. Li.^[11] Lithium insertion and extraction in LiFePO₄ cathode involves a first-order phase transition between the FePO₄ and LiFePO₄ phases. Both these phases have low electronic conductivity, and low rate of Li-ion diffusion, thus limiting the charge and discharge current density.^[11] These cause low capacity and poor power capability in LiFePO₄ batteries. LFP material has low electronic conductivity (10^{-9} to 10^{-10} S·cm⁻¹), but the conductivity can be increased by carbon coating and by decreasing the particle size.^[12] In particular, carbon-coated LiFePO₄ (c-LiFePO₄) cathodes have achieved high capacity (90% or higher of 170 mAh/g) and excellent cycling performance.^[13] Dubarry et al.^[14] studied fading mechanisms of LFP based batteries at 25 and 60°C by incremental capacity analysis, and observed that the capacity degradation at higher temperatures can be attributed to the loss of active materials or loss of lithium inventory, because of electrochemical milling. In another study on commercial Li-ion batteries with LFP cathodes, Anseán et al.^[15] cycled high power cells under multistage fast charging and standard charging procedures. The results revealed that both the charging methods caused similar ageing effects, and degradation was caused by a linear loss of lithium inventory, coupled with a less degree of loss of active material on the anode. Safari et al.^[16] examined the ageing of commercial graphite/LFP cell under cycling and storage conditions at 25 and 45°C, and the comparison of the cells aged at the same temperature revealed that the cells under cycling lose more capacity than those under OCP storage. Zhang et al.^[13] also reported capacity and power fading characteristics in prismatic LIBs with LFP cathodes at various temperatures under constant charge/discharge cycling and FUDS drive profiles. The loss of cyclable (reversible) lithium is the main reason for capacity fading, and the increased cell interfacial resistance due to the growth of solid-electrolyte interphase (SEI) layer on anode and the increased electrolyte resistance are reported as the main reasons for power fade, leading to poor discharge pulse power capability at low temperatures.

The layered Li(NiMnCo)O₂ (NMC) compounds with a hexagonal structure have received greater attention for use in LIBs due to high voltage, better stability (cycle life), higher reversible capacity (200 mAh/g in the voltage range of 2.8 to 4.6 V) and milder stability at charged state. The main problem of the NMC is the cation mixing between nickel and lithium ions, since the ionic radius of Ni²⁺ (0.69 Å) is close to that of Li⁺ (0.76 Å), resulting in the electrochemical performance deterioration.^[17] Bloom et al.^[18] studied NMC positive electrode based Li-ion cells with and without LiC₂O₄BF₂ electrolyte additive at 60% state of charge (SoC). The analysis of C/25 capacity data showed that the C/25 capacity decreases with square root of time, and the additive slowed down the rate of capacity fading. Differential voltage (dV/dQ) analysis indicated that the lithium-capacity-consuming side reaction occurring at the negative electrode caused the capacity decrease, which was like cells

with NCA. Käbitz et al.^[19] conducted a cycle and calendar life ageing study of graphite/NMC Li-ion pouch cells. SEI formation on anode was expected to be the main ageing mechanism for calendar life tests, causing a square root of time shaped ageing behavior. The analysis also shows distinct capacity loss for the cathode material at high SoC and high temperature, where SoC has a higher impact than temperature.

Typically, recycling is considered as the default end-of-life application for electric vehicle batteries. But, these batteries still have around 70–80% of their original storage capacity at the point of retirement.^[20] The reuse of the electric vehicle batteries in second-use applications following the end of their use in the vehicle may have the potential to offset the high initial cost of the batteries today. There are several grid-related applications where the second-life use of electric vehicle batteries is possible such as energy storage for renewable energy technologies like solar and wind energy, area regulation, peak load reduction and other such commercial and residential needs.^[21] The modeling based study by Sathre et al.^[20] concluded that second-life batteries in California may deliver around 15 TWh per year in 2050, which will roughly be 5% of the total electricity use in California in the same year. A model developed using several homes in Davis, California with second-life battery storage and PV arrays determined that the peak electricity demand could be reduced by 70%, while exporting less than 5% of the total energy generated from the PV array.^[22] Aziz et al.^[23] provided practical and theoretical data showing feasibility of an energy management system using a 20 kW PV panel and five EV and five retired EV batteries, both with capacity 16 kWh. In a study by Tong et al.^[24] second life lithium vehicle batteries were tested as energy storage devices, and it revealed that a 10 kWh battery and 2.16 kW PV array can provide the requirements for energy storage with 81% reduction of imported energy from the grid. Pouch format NMC/C based Li-ion cells were tested for mitigating the variability of a grid-scale PV power plant. Capacity tests at C/3 rate and Hybrid Pulse Power Capability (HPCC) tests were performed, and based on the results, lifetime of more than five years can be expected.^[25]

In the present study, cylindrical LFP and NMC based LIBs were evaluated under PHEV protocol through Federal Urban Driving Schedule (FUDS) with charge depletion (CD) mode at 50°C and <10% RH, focusing on the performance and failure mode/capacity fading analysis. In addition, second life-use of the retired batteries (after PHEV studies) was also evaluated under constant current charge/discharge cycling procedure at 50°C. Based on the XRD analysis of the cycled cathodes, the capacity fading of the LIBs is confirmed due to loss of lithium inventory.

Experimental Section

PHEV Drive Protocol

In this study, Li-ion batteries were subjected to a typical FUDS driving patterns as per the EPA protocol.^[26] FUDS protocol represents a city drive profile for light duty vehicles, having frequent stops and starts, thus including frequent acceleration and

braking. The FUDS drive cycle runs for 1369 sec with an average speed of 19.59 mph, covering 7.45 miles and the maximum speed achieved during the FUDS drive cycle is 56.7 mph.

Hybrid powertrains can run in charge-sustaining (CS), charge-depleting (CD), and blended modes, based on the SoC and torque requirements of the batteries. In most PHEVs under the CD mode, the batteries are discharged from 100 to 30% SoC. Here, the experiments were done using CD mode discharge for the batteries from 100 to 0% SoC, to accelerate the ageing process to degrade the batteries faster. Figure 1 represents the CD mode current profile

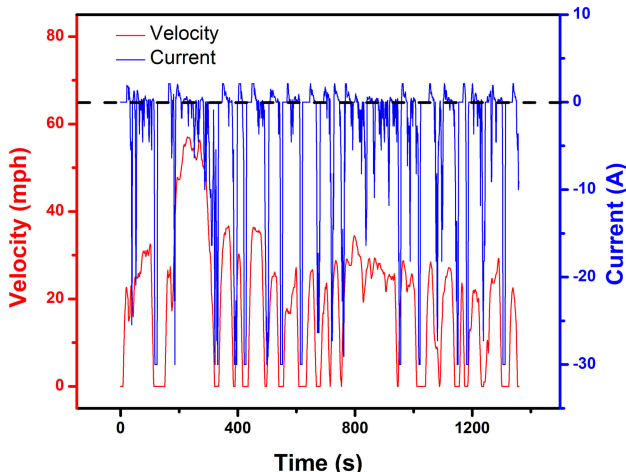


Figure 1. FUDS velocity and current profiles for PHEVs under charge-depleting mode.

based on the FUDS velocity profile, with the current scaled to a maximum value of $+/-30$ A. The detailed procedure to derive current profiles was retrieved, studied, and published by Peterson et al.^[27] The CD mode current profile scaled to $+/-20$ A was directly taken from our previous publication.^[29]

Battery Cycle-Life Tests

Three sets of battery packs (cells connected in parallel) were subjected to PHEV FUDS current loads under CD mode at elevated temperature (50°C), and a humidity level of less than 10% RH. The battery cycling protocol was automatically controlled using the schedule file of the Arbin Battery Testing system. The charge and discharge voltage cut-off values for the LFP batteries were 3.6 and 2 V, and the values were 4.2 and 2.6 V for the NMC based battery. The current profile (Figure 1) obtained using the FUDS velocity profiles was used to simulate the PHEV protocol for the LIB packs. As mentioned above, 26650 Li-ion battery packs with 2 cells connected in parallel (Battery A and B) with LFP and NMC cathodes were used, with rated capacity of 5 Ah and 8 Ah, respectively. The simulated PHEV cycle-life tests of the LIBs were carried out using the Arbin BT2000 series Battery Cycler with a current range of -20 to $+20$ A. Another battery pack, where four 18650 Li-ion cells in parallel had a rated capacity of 4.4 Ah (Battery C), and was also subjected to PHEV protocol under identical conditions. The cycling procedure was carried out in an Arbin battery cycler with a current range of -30 to $+30$ A.

The battery cycling procedure is shown schematically in the form of a flowchart in Figure 2. As seen in Figure 2, the batteries were initially charged at 1C rate up to the charge cut-off voltage, and the discharged using the FUDS current profiles after a rest time of

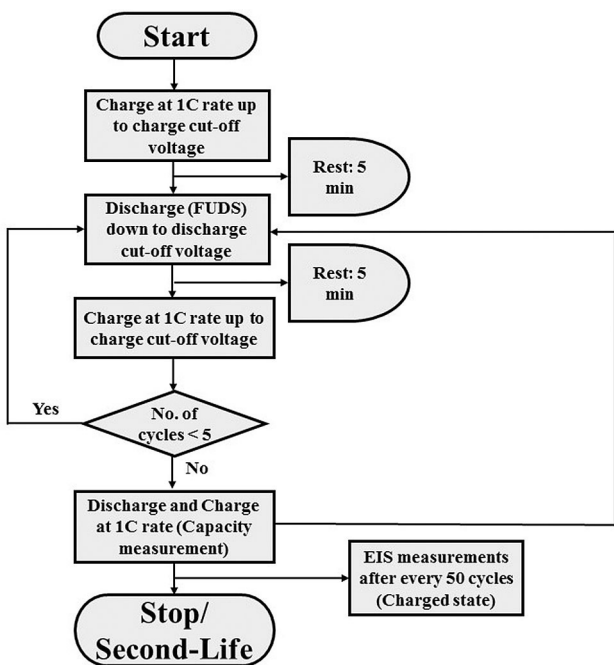


Figure 2. Flowchart for charge–discharge test procedure under PHEV driving schedule at 50°C .

5 mins. Later, batteries were charged and discharged at 1C rate. Further, impedance measurement was carried out at fully charged state (100% SoC). In the battery cycling experiments, four FUDS cycles, to discharge the batteries down to their cut-off voltage, along with one constant charge and constant discharge cycle at 1C rate is defined as one duty cycle.

Second-Life Tests

Second life batteries would play an important role in grid storage applications and as power backup system in telecom industry.^[28] After PHEV cycling, one cell out of the battery pack of two cells for each of the 26650 battery packs was used for materials characterization tests, and the other cell was subjected to second-life cycle tests. The rated capacity values for each of the 26650 Li-ion cell with LFP cathode was 2.5 Ah, and the capacity for the 26650 Li-ion cell with NMC cathode was 4 Ah. The 18650 Li-ion cells (LFP cathode) used for PHEV cycling was a pack of 4 cells. Here, two out of the four cells were used for continuing second-life tests and the other cells were used for materials analysis. For second-life testing, the batteries were evaluated at C/5 rate charge–discharge cycling procedure using the Arbin Battery Cycling equipment.

Electrochemical Impedance Spectroscopy (EIS) and XRD Analyses

EIS Analysis: Electrochemical impedance spectroscopy (EIS) measures the impedance of a system over a range of frequencies, and the frequency response of the systems reveals the properties of the system. Impedance is the opposition (resistance) to flow of alternating current (AC) in systems. EIS analysis is one of the most widely used *in situ* techniques for understanding the impedance response of electrochemical systems. It uses an AC signal to probe the impedance characteristics of a cell, by scanning the signal over a range of frequencies to generate an impedance spectrum. Theoretically, impedance spectra of LIBs consist of an inductive tail

at high frequencies, an intercept with Z_{re} axis (high-frequency resistance, HFR) or the ohmic resistance (R_1) which represents the summation of all the resistances because of electrolyte, current collectors, electrodes and connections. The semi-circular arcs in the mid frequency range can be attributed to the SEI layer and the charge transfer resistance (R_2) the electrode-electrolyte resistance. Also, the tangential line in the EIS spectra at lower frequency is due to the diffusion processes between the electrodes.^[29–31] EIS is a widely used non-invasive technique used to understand behavior of an electrochemical cell at SoCs and in different environmental conditions. EIS measurements were carried out in the frequency range 1 KHz to 10 mHz, with a voltage amplitude of 50 mV using PARSTAT-2273 Galvanostat/Potentiostat at 100% SoC with 10 mins rest after the charging in the Arbin Battery Cycler.

XRD Analysis: In order to examine the electrode materials using XRD, the LIBs after cycling studies were fully discharged and then disassembled. The anode and cathode active materials coated on copper and aluminum foils, respectively were collected using plastic knives. The active material samples were washed thoroughly in propylene carbonate solvent by sonication (for 10 minutes) to dissolve and eliminate the electrolyte (lithium salts) present. The washed samples were vacuum dried at 50 °C overnight, after rinsing in ethanol, for XRD analysis. XRD examination of the powdered electrode active material samples was carried out using a PANalytical X'Pert Pro diffractometer using Cu target (CuK α radiation of 1.54 Å) from 20 to 65 degrees (2 θ) at a very slow scan rate (0.005 degree per second) and the patterns were analyzed using Highscore Plus software.

Equivalent Circuit Modeling

EIS measurements are used for arriving at the HFR values, which are denoted by R_1 in the model. Equivalent circuit modeling is necessary to obtain information on the other circuit elements. Hence, equivalent circuit were developed using EC lab to model the circuit behavior with charge transfer resistance (R_2) values.

2. Results and Discussions

2.1. Capacity Fading Under PHEV Cycling

Figure 3a,b shows the discharge profiles of the batteries under CD mode at the beginning and the end of PHEV cycling. Similarly, the charging profiles (1C rate) of all the batteries at the beginning and end of PHEV cycling are shown in Figures 3c. As seen in Figures 3a and 3b, it takes nearly 120 minutes for battery A (26650 NMC-based) to discharge to 2 V while it takes about 160 minutes for battery B (26650 NMC-based) to discharge to 2.6 V, and battery C (18650 LFP-based) takes approximately 50 minutes to discharge to 2 V. It is also very clearly seen that the voltage profile for batteries A and C (LFP based) is flatter compared to the voltage profile of battery B. Accelerated cycling tests showed different capacity fading characteristics in the batteries.

Figure 4a–c shows the cyclability data for the batteries tested under CD mode at elevated temperature (50 °C) and low humidity values (<10% RH). Batteries A and B underwent 800

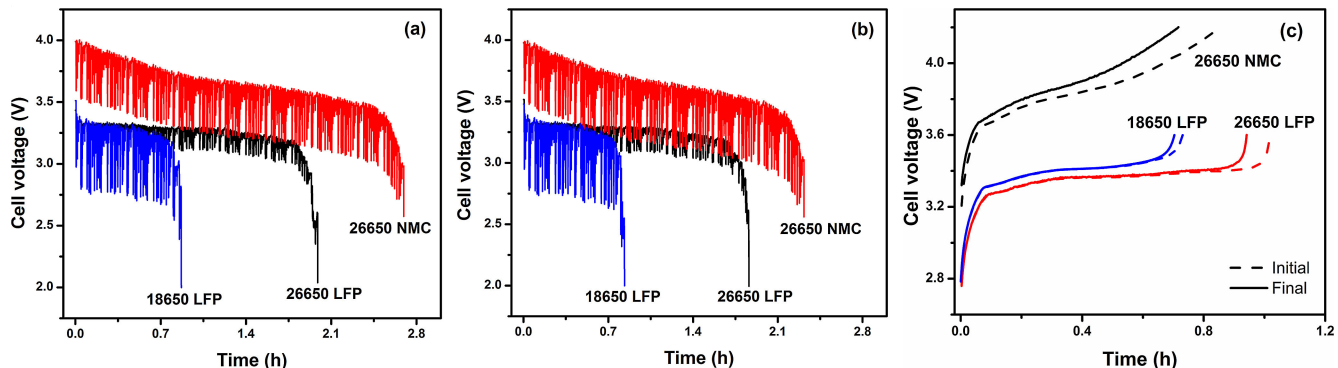


Figure 3. FUDS discharge profiles (a) initial (b) final (after PHEV cycling) and (c) initial and final charge profiles at 1C rate.

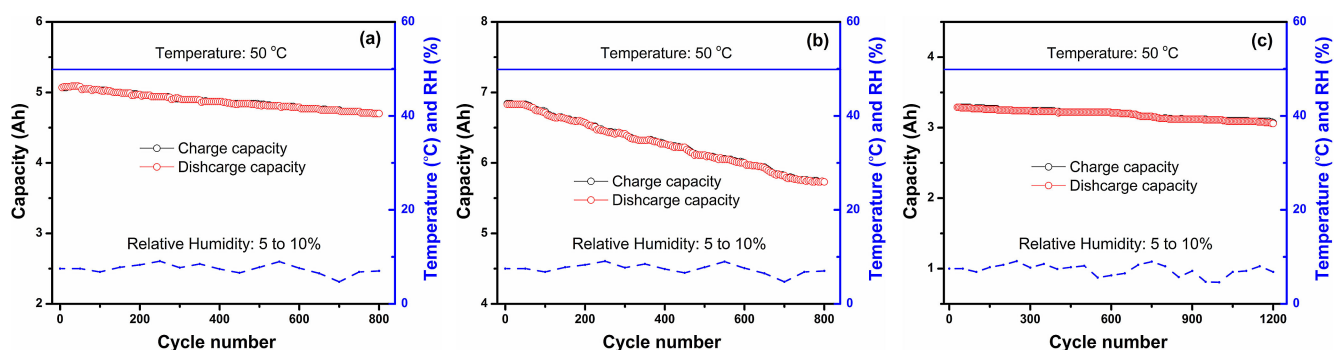


Figure 4. Cyclability data for (a) 26650 (LFP cathode), (b) 26650 (NMC cathode) and (c) 18650 (LFP cathode) based Li-ion cells.

cycles, while the battery C had 1200 cycles, and the tests were carried out continuously for 6 months.

As shown in Table 1, capacity drop per 100 cycles at high temperature was approximately 1, 2, and 0.5% for CD mode in batteries A, B and C, respectively. After 800 PHEV cycles, around 8% capacity degradation was seen in 26650 LFP-based Li-ion cells (battery A), and 16% degradation was observed in 26650 NMC-based Li-ion cells (battery B). Similarly, in 18650 LFP-based Li-ion cells (battery C), 6.5% decrease in capacity is observed after 1200 PHEV cycles. It is evident that the capacity fading rate is more dominant in NMC based cells compared to LFP based cells.

Figure 5a–c compared the discharge performance after different cycle numbers for the three battery packs used. Also, differential voltage (dV/dQ) values were calculated based on the discharge performance and Figure 5d–f shows dV/dQ curves for battery A, B and C, respectively. In all the batteries, the differential voltage profiles shift towards the left in comparison with that of the initial performance, due to loss of lithium ions. Hence, as per references,^[13,14,18] it can be summarized that the capacity fading mechanism in both the

batteries is due to loss of lithium inventory (LLI) with different fading rates.

2.2. EIS Analysis

Figure 6a–c shows the impedance spectra for the Li-ion battery packs at 100% SoC during PHEV cycling at various cycles under CD mode at 50 °C. It is seen that all the patterns show an inductive tail at higher frequency. The semi-circular arcs in the mid frequency range can be attributed to the SEI layer and the charge transfer resistance (R_2), which corresponds to the electrode-electrolyte resistance.^[31,32] As clearly observed, the HFR for the batteries increases (intercepts on the Z_{re} axis) with cycling. It is interesting to note that initial impedance exhibited by NMC cathode based cells is much higher compared to that of the LFP. However, on cycling (over 800 cycles) LFP (batteries A and C in Table 1) based cells show higher increase in impedance (~54%) compared to that with NMC (battery B in Table 1) based cells (16%) from their respective initial HFR values. In addition, the ionic resistance is also found to increase

Table 1. Type and performance of LIBs under PHEV and second-life evaluation.

Battery Sample	Type	PHEV test protocol			Second-life test protocol		
		Number of cycles	Capacity decrease per 100 cycles [%]		Number of cycles	Capacity decrease per 100 cycles [%]	
A	26650 Li-ion (5 Ah, LFP cathode)	800	0.9		200	2.7	
B	26650 Li-ion (8 Ah, NMC cathode)	800	2.01		205	2.06	
C	18650 Li-ion (4.4 Ah, LFP cathode)	1200	0.58		217	1.6	

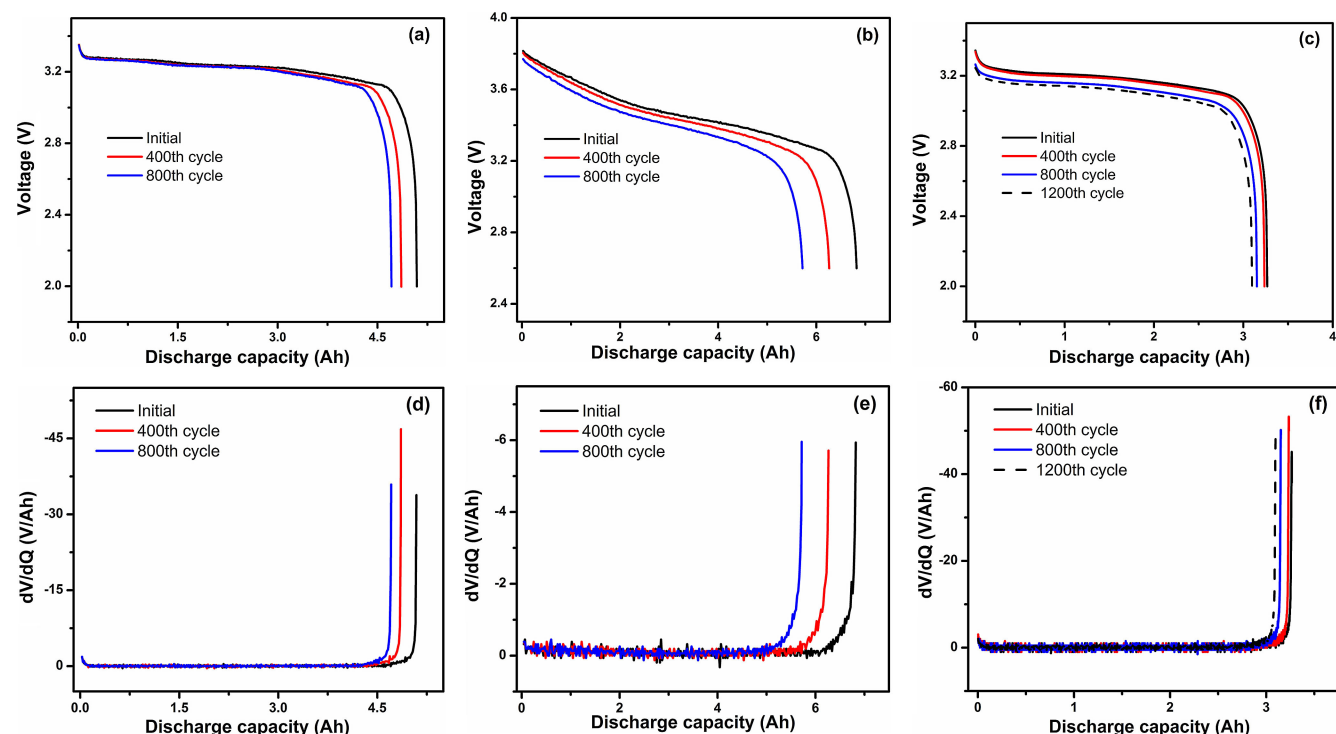


Figure 5. Discharge profiles (every 400 cycles) for (a) 26650 (LFP cathode), (b) 26650 (NMC cathode) and (c) 18650 (LFP cathode); and differential voltage profiles for (d) 26650 (LFP cathode), (e) 26650 (NMC cathode) and (f) 18650 (LFP cathode) based Li-ion cells.

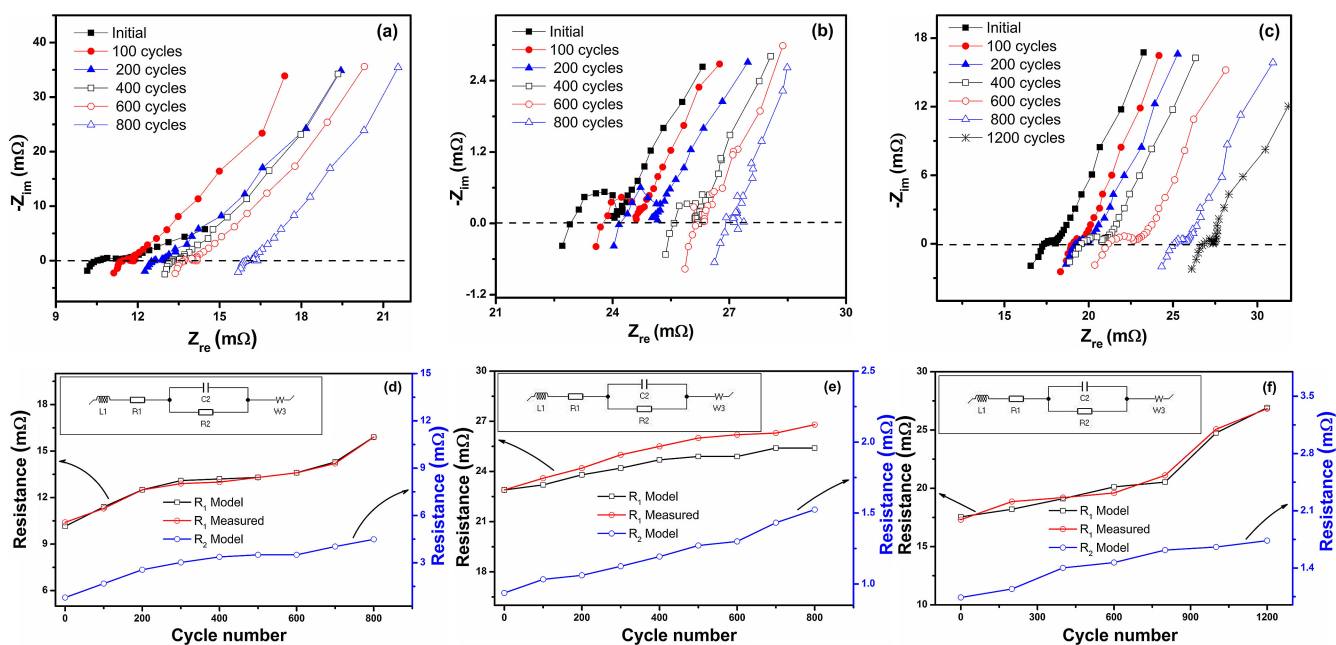


Figure 6. EIS Nyquist plots for (a) 26650 (LFP cathode), (b) 26650 (NMC cathode), and (c) 18650 (LFP cathode) in fully charged state during PHEV cycling (various cycle numbers); and HFR and charge transfer resistance values with cycling for (d) 26650 (LFP cathode), (e) 26650 (NMC cathode), and (f) 18650 (LFP cathode) based Li-ion cells. The insets in (d), (e), and (f) are the equivalent circuits.

with cycling as there is a slight increase in diameter of spectra with cycling (Figure 6a-c). Figures 6d-f shows the HFR and charge transfer resistance values with cycling, along with their corresponding equivalent circuits (consisting of inductor, resistor along with CPE elements) as insets for the LIBs with LFP as well as NMC cathodes. Rise in the HFR with cycling is an indication of passivation (clogging of micro-pores) of the negative electrode and the decomposition of the electrolyte, leading to loss of lithium inventory and phase transformation of cathodes.^[33] The increase in charge transfer resistance in NMC and LFP based cells on cycling at higher temperature is possibly due to deterioration of cell kinetics.^[34] As seen from Figures 6d-f, the rate of increase in HFR (R_1) is relatively higher compared to that of the charge transfer resistance (R_2) in the LIBs, which shows that the capacity fading due to lithium loss is dominant as compared to the power fading due to the charge transfer resistance. Overall, contribution of HFR is higher in

both LFP and NMC cathodes compared to charge transfer resistance with cycling/ageing.

2.3. Second-Life Evaluation

To offset the high initial cost of the LIBs used in electric vehicles, second life-use of the retired batteries is gaining importance in power back-up systems and grid storage applications. Hence, this possibility was also examined by evaluating the LIBs under constant current charge/discharge cycling at 50 °C, after PHEV protocols. As seen from the cyclability data in Figure 7a,b, ~4.9% and 4.4% capacity reduction (from the value at the beginning of second-life cycling) was observed after 200 second-life cycles for the batteries A and B, respectively. It is interesting to note that the capacity degradation at a constant current charge–discharge rate (C/5) is higher in case of the LPF cathode based battery compared to that with NMC cathode.

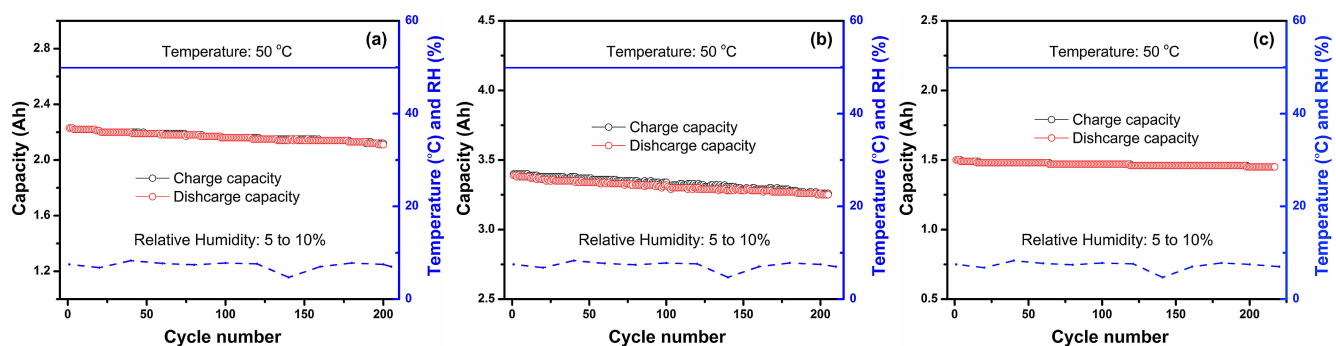


Figure 7. Second-life cyclability data for (a) 26650 (LFP cathode), (b) 26650 (NMC cathode) and (c) 18650 (LFP cathode) based Li-ion cells, after PHEV cycling.

This can be attributed to the higher initial capacity value due to the higher energy density of NMC cathode material, and the lower discharge rate ($C/5$) used for charge–discharge cycling. In battery C (Figure 7a), there was a 3.4% capacity reduction after 215 second-life charge/discharge cycles at $C/5$ rate. The cyclability data for all the LIBs during second-life testing after PHEV protocol is very attractive and can be useful for large scale energy storage or residential or load leveling applications.

2.4. XRD Analysis

XRD experiments were carried out on the cycled LFP and NMC cathodes for analyzing phase change during both PHEV and second-life cycling. Figure 8a–c shows the XRD patterns for fresh (uncycled) and cycled cathode materials (after PHEV and second-life tests) for battery A, B, and C, respectively. In Figure 8a, sharp intense peaks are observed for the triphylite (LiFePO_4 , ICDD Card #01-072-7845), and no heterosite peaks (FePO_4 , ICDD Card #00-029-0715) were observed for the LFP cathode materials. Maximum intensity peak for characteristic LiFePO_4 was at $2\theta = 35.5\text{--}36$ degrees for all the samples and it had Miller indices (hkl) of (311) and was similar to the ones reported in the literature by Padhi and co-workers^[11]. In Figure 8b, the XRD patterns for the NMC cathode samples after PHEV cycling are compared with that of the fresh (uncycled) cathode sample. The fresh and cycled cathode materials show intense peaks of $\text{Li}(\text{NiMnCo})\text{O}_2$ in the range $2\theta = 44.4\text{--}44.8$ degrees. Also, the NMC cathode patterns could be perfectly matched and indexed as per the standard $\text{Li}(\text{NiMnCo})\text{O}_2$ pattern (ICDD Card # 00-56-0147). The fresh and cycled cathodes in batteries A and B had lattice parameter values (a, b, c)

(calculated using Rietveld Analysis) closely matching with the standard patterns for LiFePO_4 and $\text{Li}(\text{Ni–Mn–Co})\text{O}_2$, respectively.

As seen from Table 2, no phase change in the cathode samples during cycling was observed. Based on the Rietveld Analysis, after second-life tests, there is a slight distortion in the crystal structure of the sample, and the crystal structure changes from rhombohedral to hexagonal with similar lattice parameters. In case of battery C (Figure 8c), the fresh electrode has a maximum intensity LiFePO_4 peak at $2\theta = (35.5\text{--}36.0$ degrees), but the cathode material after PHEV and second-life cycling had peaks corresponding to FePO_4 (marked by #102, 103, and 104). Hence, we can see that there is a change of phase from LiFePO_4 to FePO_4 in battery C, which is mainly due to loss of Li ions. As seen in Table 2, this is also evident from the significantly different lattice parameters of the cycled cathode samples as compared to the standard LiFePO_4 pattern, and reveals a mixture of LiFePO_4 and FePO_4 in the sample. Also, the decrease in the crystallite size (see Table 2) for the cathode samples for all the batteries can be attributed electrochemical milling or dissolution of active materials,^[14] leading to loss of Li ions.

The XRD analysis reveals that there is no significant change in the phase structure of the electrodes in battery A and B after 800 PHEV cycles, while after 1200 cycles in battery C, FePO_4 phase is observed along with LiFePO_4 phase, confirming loss of Li^+ ions during intercalation. Even after 200 second-life cycles post PHEV cycling, cathode active materials in batteries A and B did not reveal any phase change. The present study clearly demonstrates the possibility of employing LIBs for various second-life applications after they retire from PHEV or EV use.

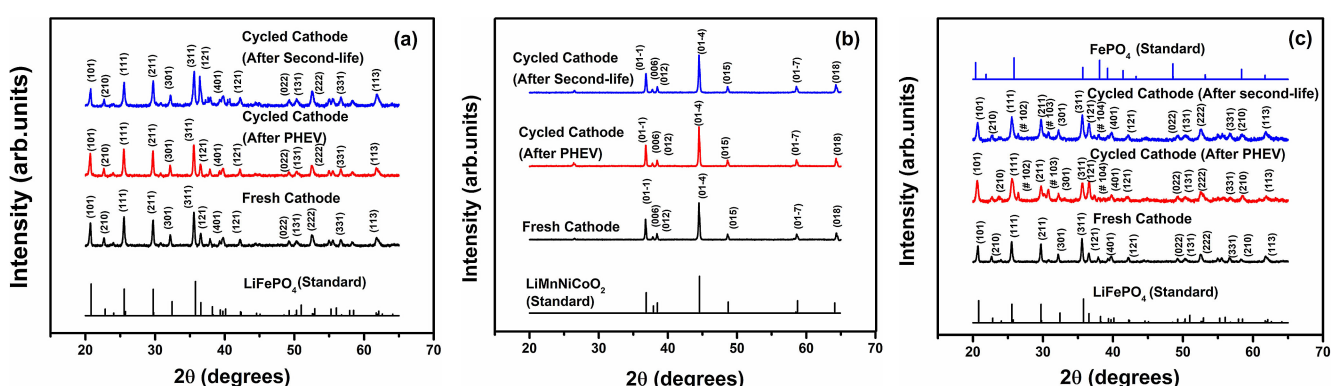


Figure 8. XRD patterns of cycled (after PHEV and second-life) cathodes for (a) 26650 (LFP cathode), (b) 26650 (NMC cathode) and (c) 18650 (LFP cathode) along with their respective fresh cathode samples.

Table 2. Rietveld analysis results and particle size values for the fresh and cycled cathodes from the XRD patterns.

ID	Battery type	Cathode sample	Space group	Lattice parameters (a, b, c) [\AA]	Particle size [nm]
A	26650 Li-ion (LFP cathode)	Fresh	<i>Pnma</i>	10.3222, 5.9830, 4.6799	58
		After second-life cycling	<i>Pnma</i>	10.05, 6.01, 4.73	54
B	26650 Li-ion (NMC cathode)	Fresh	<i>R3m</i>	2.8579, 2.8579, 14.2236	71
		After second-life cycling	<i>R3m</i>	2.8569, 2.8569, 14.287	70
C	18650 Li-ion (LFP cathode)	Fresh	<i>Pnma</i>	10.3222, 5.9830, 4.6799	58
		After second-life cycling	<i>Pnma</i>	10.295, 5.989, 4.705	33

3. Conclusions

LIBs with LFP and NMC cathodes subjected to charge-depleting operating mode under the FUDS drive cycle (discharge current: 20 A) showed 8% and 16% capacity decrease, respectively after 800 PHEV cycles. In 18650 Li-ion cells (LFP cathode), there was a 6.5% decrease in capacity after 1200 PHEV cycles, with the discharge current scaled to maximum value of $+/-30$ A. The major finding of the study was that LIBs with NMC cathodes showed twice the capacity degradation as compared to that with LFP cathodes under identical operating conditions, restating the fact that LFP based batteries have higher cycle life characteristics compared to other LIB chemistries. The high frequency resistance and the charge transfer resistance are seen to increase with cycling, and it can be attributed to the loss of Li^+ ions because of SEI layer formation. Further, the LIBs evaluated for second-life use by performing constant current charge/discharge cycling at a C/5 rate, showed less than 5% capacity loss over 200 cycles with both LFP and NMC cathodes. Detailed Rietveld analysis carried out on the XRD patterns for both the LFP and NMC cathodes based 26650 LIBs before and after PHEV (800 PHEV cycles) and second-life cycling (200 second-life cycles) did not show any evidence of phase change. However, the XRD analysis of 18650 LIBs with LFP cathode revealed phase change from LiFePO_4 to FePO_4 due to cycling after PHEV and Second-life tests.

Acknowledgements

The authors would like to acknowledge financial support from Salt River Project, Phoenix, AZ through Conservation and Renewable Energy Collaboratory.

Conflict of Interest

The authors declare no conflict of interest.

Keywords: Capacity degradation • Cycle-life test • Energy storage • Lithium-ion batteries • Plug-in hybrid electric vehicles

- [1] IPCC, *Summary for Policymakers and Technical Summary*. 2014.
- [2] A. Sakti, J. J. Michalek, E. R. H. Fuchs, J. F. Whitacre, *J. Power Sources*. **2015**, *273*, 966–980.
- [3] Overview of Greenhouse Gases [Online] Available: <https://www.epa.gov/ghgemissions/overview-greenhouse-gases#carbon-dioxide>.

- [4] USABC, *Electric Vehicle Battery Test Procedures – Rev. 2*. **1996**, 129.
- [5] A. Emadi, Y. J. Lee, K. Rajashekara, *IEEE Trans. Ind. Electron.* **2008**, *55*, 2237–2245.
- [6] T. Yuksel, S. Litster, V. Viswanathan, J. J. Michalek, *J. Power Sources*. **2017**, *338*, 49–64.
- [7] H. Budde-Meiwes, J. Drillkens, B. Lunz, J. Muennix, S. Rothgang, J. Kowal, D. U. Sauer, *Proc. Inst. Mech. Eng. Part D J. Automob. Eng.* **2013**, *227*, 761–776.
- [8] DOE VTO - Batteries [Online] Available: <https://www.energy.gov/eere/vehicles/batteries>.
- [9] J. Axsen, A. F. Burke, K. S. Kurani, *Electric and Hybrid Vehicles*. **2010**, ISBN:978-0-444-53565-8, 405–427.
- [10] N. Nitta, F. Wu, J. T. Lee, G. Yushin, *Mater. Today*. **2015**, *18*, 252–264.
- [11] J. B. Goodenough, A. K. Padhi, K. S. Nanjundaswamy, *J. Electrochem. Soc.* **1997**, *144*.
- [12] K. Striebel, J. Shim, V. Srinivasan, J. Newman, *J. Electrochem. Soc.* **2005**, *152*, A664.
- [13] Y. Zhang, C. Y. Wang, X. Tang, *J. Power Sources*. **2011**, *196*, 1513–1520.
- [14] M. Dubarry, B. Y. Liaw, M. S. Chen, S. S. Chyan, K. C. Han, W. T. Siec, S. H. Wu, *J. Power Sources*. **2011**, *196*, 3420–3425.
- [15] D. Anseán, M. Dubarry, A. Devie, B. Y. Liaw, V. M. García, J. C. Viera M. González, *J. Power Sources*. **2016**, *321*, 201–209.
- [16] M. Safari, C. Delacourt, *J. Electrochem. Soc.* **2011**, *158*, A1123.
- [17] C. M. Julien, A. Mauger, K. Zaghib, H. Grout, *Inorganics*. **2014**, *2*, 132–154.
- [18] I. Bloom, L. K. Walker, J. K. Basco, D. P. Abraham, J. P. Christophersen, C. D. Ho, *J. Power Sources*. **2010**, *195*, 877–882.
- [19] S. Käbitz, J. B. Gerschler, M. Eckerac, Y. Yurdagel, B. Emmermacher, D. André, T. Mitsch, D. U. Sauer, *J. Power Sources*. **2013**, *239*, 572–583.
- [20] R. Sathre, C. D. Scown, O. Kavvada, T. P. Hendrickson, *J. Power Sources*. **2015**, *288*, 82–91.
- [21] J. Neubauer, A. Pesaran, *J. Power Sources*. **2011**, *196*, 10351–10358.
- [22] M. A. Kootstra, S. Tong, J. W. Park, *Int. J. Energy Res.* **2015**, *39*, 825–841.
- [23] M. Aziz, T. Oda, T. Kashiwagi, *Energy Procedia*. **2015**, *75*, 1938–1943.
- [24] S. Tong, T. Fung, J. W. Park, *IEEE Int. Conf. Smart Grid Commun.* **2015**, 325–330.
- [25] M. Swierczynski, D. I. Stroe, E. M. Laserna, E. Sarasketa-Zabala, J. M. Timmermans, S. Goutam, R. Teodorescu, *ECS Trans.* **2016**, *74*, 55–62.
- [26] EPA UDDS [Online] Available: <https://www.epa.gov/emission-standards-reference-guide/epa-urban-dynamometer-driving-schedule-udds>
- [27] S. B. Peterson, J. Apt, J. F. Whitacre, *J. Power Sources*. **2010**, *195*, 2385–2392.
- [28] A. Opitz, P. Badami, L. Shen, K. Vignarooban, A. M. Kannan, *Renew. Sustain. Energy Rev.* **2017**, *68*, 685–692.
- [29] P. Badami, A. Opitz, L. Shen, R. Vaidya, A. Mayyas, K. Knoop, A. Razdan, A. M. Kannan, *Int. J. Hydrogen Energy*. **2017**, *42*, 12396–12404.
- [30] D. Andre, M. Meiler, K. Steiner, H. Walz, T. Soczka-Guth, D. U. Sauer, *J. Power Sources*. **2011**, *196*, 5349–5356.
- [31] D. Andre, M. Meiler, K. Steiner, C. Wimmer, T. Soczka-Guth, D. U. Sauer, *J. Power Sources*. **2011**, *196*, 5334–5341.
- [32] K. Ozawa, *Solid State Ionics*. **1994**, *69*, 212–221.
- [33] J. Vetter, P. Novák, M. R. Wagner, C. Veit, K. C. Möller, J. O. Besenhard, M. Winter, M. Wohlfahrt-Mehrens, C. Vogler, A. Hammouche, *J. Power Sources*. **2005**, *147*, 269–281.
- [34] S. S. Zhang, *J. Power Sources*. **2006**, *161*, 1385–1391.

Manuscript received: January 23, 2018
Version of record online: April 25, 2018